Article

Developmental Cell

Signaling Dynamics Control Cell Fate in the Early *Drosophila* Embryo

Graphical Abstract

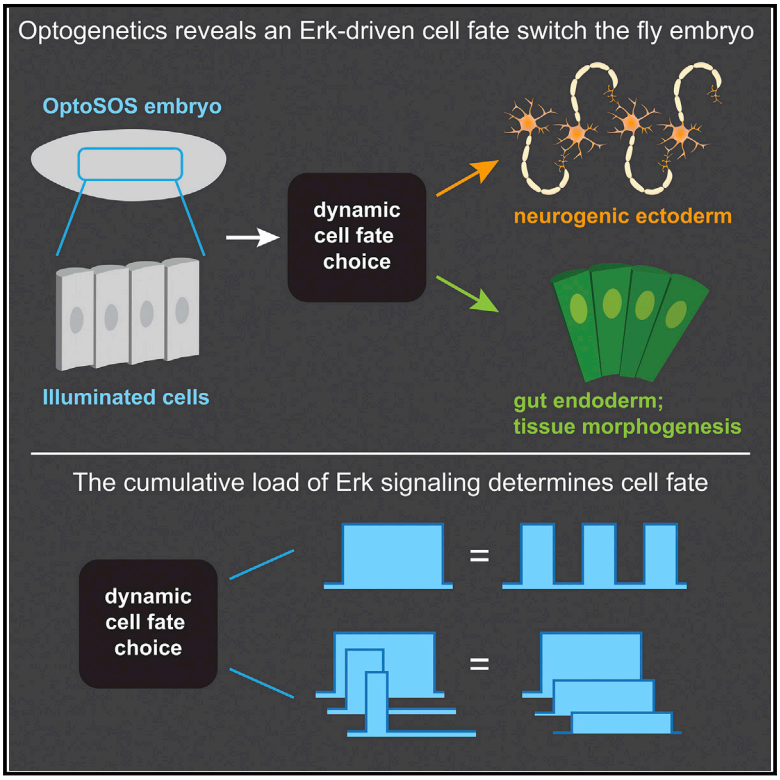

Highlights

- Optogenetic Erk activation drives multiple differentiation and morphogenetic events
- Light-activated Erk is sufficient to switch cells between endoderm and ectoderm fates
- The total dose of Erk activity, not amplitude or duration, dictates cell responses
- Target gene responses to Erk range from gradual accumulation to sharp activation

Authors

Heath E. Johnson, Jared E. Toettcher

Correspondence

toettcher@princeton.edu

In Brief

Johnson and Toettcher use optogenetics to dissect Erk-dependent responses in the early *Drosophila* embryo, discovering an endoderm/ectoderm cell fate switch that depends on the dynamics of Erk activity.

Johnson & Toettcher, 2019, Developmental Cell *48*, 361–370
February 11, 2019
https://doi.org/10.1016/j.devcel.2019.01.009

CellPress

Developmental Cell
Article

Signaling Dynamics Control Cell Fate in the Early *Drosophila* Embryo

Heath E. Johnson[1] and Jared E. Toettcher[1,2,*]
[1]Department of Molecular Biology, Princeton University, Princeton, NJ 08544, USA
[2]Lead Contact
*Correspondence: toettcher@princeton.edu
https://doi.org/10.1016/j.devcel.2019.01.009

SUMMARY

The Erk mitogen-activated protein kinase plays diverse roles in animal development. Its widespread reuse raises a conundrum: when a single kinase like Erk is activated, how does a developing cell know which fate to adopt? We combine optogenetic control with genetic perturbations to dissect Erk-dependent fates in the early *Drosophila* embryo. We find that Erk activity is sufficient to "posteriorize" 88% of the embryo, inducing gut endoderm-like gene expression and morphogenetic movements in all cells within this region. Gut endoderm fate adoption requires at least 1 h of signaling, whereas a 30-min Erk pulse specifies a distinct ectodermal cell type, intermediate neuroblasts. We find that the endoderm-ectoderm cell fate switch is controlled by the cumulative load of Erk activity, not the duration of a single pulse. The fly embryo thus harbors a classic example of dynamic control, where the temporal profile of Erk signaling selects between distinct physiological outcomes.

INTRODUCTION

One of the great mysteries of animal development is how a small number of intracellular signals can be reused at different positions and times to coordinate a wide range of cell fate decisions. A classic paradigm for this one-to-many mapping is the idea of a morphogen, a substance whose concentration varies with embryonic position and where different concentrations are sufficient to induce different cell fates (Gurdon et al., 1998). Alternatively, cell fates may be specified by combinatorial control: the spatial overlap between particular combinations of patterning cues (Rahimi et al., 2016). A third model, dynamic control, holds that a single signal could select among cellular responses based on features such as the amplitude, duration, or frequency of pathway activation (Imayoshi et al., 2013; Purvis and Lahav, 2013). Although all three paradigms have been proposed to explain cell fate decisions, directly demonstrating which paradigm underlies particular developmental decisions has been extremely challenging. Researchers typically lack the ability to vary a single feature, such as the concentration, duration, or spatial range of a signal, while holding others constant.

Here, we set out to dissect cell fate control in a model developmental context: the Erk-dependent control of cellular responses in the early *Drosophila* embryo. Two factors make the early embryo ideal for such a study. First, Erk activity is required for cells to adopt distinct fates at three different positions (Figure 1A). Erk activation by the Torso receptor patterns head structures at the anterior pole and gut endoderm at the posterior pole, whereas Erk activation by epidermal growth factor receptor (EGFR) on the embryo's lateral surface is required to form intermediate neuroblasts, a subpopulation of neuronal progenitor cells. Second, we have previously shown that Erk signaling can be precisely controlled using optogenetics, enabling one to directly test how specific signal features map to gene expression and cell fate (Bugaj et al., 2018; Johnson et al., 2017; Wilson et al., 2017; Toettcher et al., 2013).

By combining optogenetic stimuli with classic genetic perturbations, we find that different thresholds of Erk signaling trigger cells to adopt posterior or lateral fates. High, sustained Erk activity induces gut endoderm differentiation, defined by expression of posterior genes and morphogenetic movements during gastrulation. This decision can be triggered at all but the most anterior positions in the embryo, where it is inhibited by Bicoid (Bcd). In contrast, a 30-min pulse of Erk activity expands the population of *ind*-expressing neurogenic ectoderm cells. Systematically varying the blue light stimulus reveals that differentiation into gut endoderm and neurogenic ectoderm is triggered by the total integrated dose of Erk activity, not other signal parameters such as the amplitude, duration or time of light delivery. We propose that Erk dose may be sensed by a two-step accumulator-and-thresholder mechanism and find evidence that the induction of distinct Erk target genes reflects these two operations.

RESULTS

Light-Activated Erk "Posteriorizes" the Embryo, Profoundly Disrupting Tissue Morphogenesis

We first sought to characterize the molecular and phenotypic consequences of high levels of Erk signaling throughout the early embryo. To do so, we took advantage of the OptoSOS system, in which exposure to modest intensities of blue light (0.5–2 mW/cm^2) induces Erk phosphorylation to 150%–200% of the maximum level reached in wild-type embryos within minutes at all positions in the embryo (Johnson et al., 2017). This result is different from the modest increase in Erk phosphorylation induced by gain-of-function mutations in the pathway (Figures S1A–S1C), possibly as a result of feedback inhibition that is

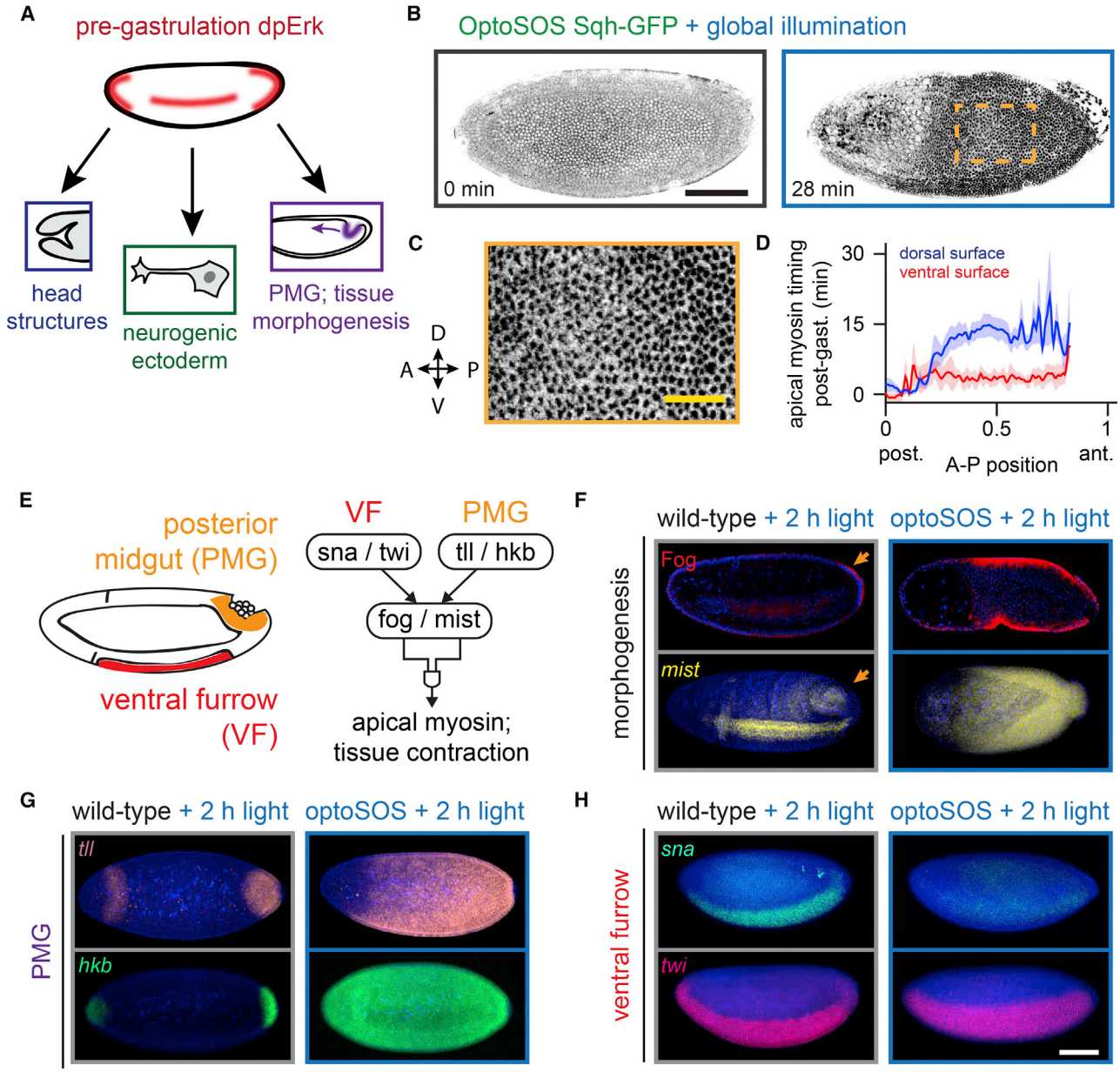

Figure 1. Optogenetic Erk Signaling Induces Gut Endoderm Gene Expression and Tissue Morphogenesis

(A) Erk activity is present at 3 locations within the blastula and coordinates distinct fates. Of these, only the posterior normally undergoes apical constriction and invagination at the start of gastrulation.

(B) Maximum-projected images from an OptoSOS-SqhGFP embryo under continuous blue light during nuclear cycle 14 (left) and during gastrulation (right). Scale bar, 100 μm. Dark regions indicate apical myosin localization (see also Video S2).

(C) Detail of boxed region from (B), showing a uniform distribution of myosin puncta across the embryo surface. Scale bar, 30 μm.

(D) Time of initial apical myosin appearance as a function of anteroposterior (A–P) and dorsoventral (D–V) position from 5 individual OptoSOS embryos.

(E) Schematic of the genetic network controlling tissue contractility in the ventral furrow and posterior midgut.

(F–H) RNA fluorescence in situ hybridization (FISH) for *mist* (F), *tll*/*hkb* (G), and *sna*/*twi* (H) and immunostaining for Fog (F) in gastrulating histone-GFP ("wild-type") and OptoSOS embryos. All embryos were illuminated for 2 h prior to fixation. Scale bar, 100 μm.

triggered by long-term pathway activation in these mutants (Goyal et al., 2017). Bright-field imaging of gastrulating OptoSOS embryos after light stimulation revealed that these embryos exhibited profound morphogenesis defects (Johnson et al., 2017), but the precise nature of these defects has not yet been determined.

To better characterize the morphogenesis phenotype of global Erk activation, we set out to image tissue movements in gastrulating OptoSOS embryos at single-cell spatial resolution. We generated OptoSOS embryos that expressed a fluorescent myosin light chain, Sqh-GFP, which redistributes to the apical surface of invaginating cells during gastrulation (Martin et al.,

2009; Royou et al., 2002). Dark-incubated OptoSOS-SqhGFP embryos gastrulated normally, exhibiting apical myosin redistribution in two tissues that normally invaginate, the ventral furrow (VF) and at the posterior pole (Video S1; Figure S2A). In contrast, OptoSOS-SqhGFP embryos exposed to 2 h of saturating blue light (1 mW/cm^2 at 450 nm) massively expanded the domain of apical myosin localization across the majority of the embryo (Figures 1B and S2B; Videos S2 and S3). We observed apical myosin appearing in puncta over the entire contractile domain without any cell-sized gaps (Figure 1B; inset shown in Figure 1C). To assess whether the decision to contract was cell-autonomous or could be propagated between cells, we stimulated OptoSOS-SqhGFP embryos with a narrow, 8-cell-wide stripe of light at the mid-embryo (Figure S2C, Video S3). We found that light stimulation only induced apical myosin and constriction within the stimulated region without propagating outwards from regions of Erk stimulation, unlike the recent observation of EGFR-driven contractility waves in the tracheal placode (Nishimura et al., 2007).

To assess the spatiotemporal dynamics of Erk-induced tissue morphogenesis, we quantified apical myosin accumulation as a function of position and time in five stimulated OptoSOS embryos (see STAR Methods and Figures S2D–S2F for details). Apical myosin appeared at all but the anterior-most positions, covering 88% of the total embryo. The timing of contraction varied with position: we observed a posterior-to-anterior wave of myosin recruitment and cell movement that was slower and more pronounced on the dorsal than ventral surface (Figure 1D). These differences in timing persisted despite the fact that blue light was simultaneously delivered to the entire embryo. Our observations begin to paint a picture for Erk-induced cell fate determination in the early embryo. Contraction is triggered only in illuminated cells (Figure S2C), and all illuminated cells exhibit apical myosin localization without gaps (Figure 1C). These data suggest that within the posterior 88% of the embryo, Erk is both necessary and sufficient to trigger contractile cell fates. However, while the decision to contract is Erk-dependent, its timing is position specific and set independently of Erk (Figure 1D).

We reasoned that Erk-induced contractility may reflect the ectopic formation of a tissue that normally contracts during gastrulation: the VF or posterior midgut (PMG) (Figure 1E). In both cases, tissue contractility is thought to be driven by the localized expression of folded gastrulation (*fog*) and *mist*, a secreted ligand and its cognate G protein-coupled receptor (GPCR) (Manning et al., 2013; Dawes-Hoang et al., 2005). Although *fog* and *mist* are involved in both VF and PMG movements, their expression in the VF is regulated by *snail* (*sna*) and *twist* (*twi*) and in the PMG by *tailless* (*tll*) and *huckebein* (*hkb*).

To test whether Erk triggers the expansion of VF- or PMG-like tissue, we stained light-stimulated OptoSOS embryos for the molecular hallmarks of contractility and tissue identity (For these and other immunofluorescence experiments, histone-GFP embryos were illuminated and stained alongside OptoSOS embryos as controls for the non-specific effects of blue light illumination; see Figures 1F–1H.). We found that the domains of *Fog* protein and *mist* mRNA expression exactly overlapped the light-stimulated contractile domain (Figure 1F). They also matched a concomitant expansion in the domain of PMG gene expression: *tll* expression was expanded to match the contractile domain, with *hkb* expression extending even further to the anterior pole (Figure 1G). In contrast, VF markers were either unaffected (in the case of *twi*) or eliminated (*sna*)—data which are consistent with the reported repression of *sna* by *hkb* (Figure 1H) (Reuter and Leptin, 1994). We also did not observe VF invagination in regions of OptoSOS embryos that were exposed to high light doses; this may be partially due to the loss of Snail expression and partially due to the global expression of *Fog* and *Mist* preventing local invagination just along the furrow.

These results can be readily interpreted in the current model of terminal signaling, which already holds that Erk signaling is necessary for posterior specification (Schüpbach and Wieschaus, 1986). We additionally find that Erk activity is sufficient to drive cells to adopt a contractile, posterior fate at all but the anterior-most positions in the embryo. This sufficiency is masked in gain-of-function mutants in Erk signaling (e.g., MEK F53S and Tor D4021), which only partially expand the posterior contractile domain and posterior gap gene expression, likely as a result of Erk signaling that is not fully activated in these mutants (Figure S1) (Goyal et al., 2017; de las Heras and Casanova, 2006; Grimm et al., 2012).

Light-Triggered Posterior Fates Are Blocked by Bcd at the Anterior Pole

Even in globally illuminated OptoSOS embryos, posteriorization fails to occur at the anterior pole. This result mirrors normal development, where high levels of Bcd at the anterior pole are required for the formation of anterior structures; indeed, *bcd* mutant embryos exhibit mirror-image posterior invaginations during gastrulation (Driever et al., 1990). These observations suggest that in the absence of Bcd, global OptoSOS activation may lead to posterior fates and contractility at all positions across the embryo (Figure 2A). To test this prediction, we generated embryos from OptoSOS mothers that are also homozygous for the *bcd*^{E1} loss-of-function allele (termed OptoSOS-*bcd*; for strain details see STAR Methods) and compared their gastrulation to OptoSOS embryos using differential interference contrast (DIC) microscopy.

OptoSOS embryos with functional Bcd contracted everywhere but the anterior pole, leading to the flow of yolk toward the anterior pole and a thinning of the epithelial monolayer there (Figure 2B; Video S4, top). In contrast, blue-light-illuminated OptoSOS-*bcd* embryos exhibited uniform, isotropic contraction during gastrulation (Figure 2C; Video S4, bottom). Normally, the asymmetric contractility of OptoSOS embryos leads to a massive anterior-to-posterior movement of cells and posterior-to-anterior flow of yolk. In contrast, the synchronized, isotropic contraction observed in OptoSOS-*bcd* embryos suppressed virtually all of these flows and movements. These embryos were still subjected to strong compressive forces, as many OptoSOS-*bcd* embryos popped, ejecting yolk and cells out of one or both poles (Video S5). We thus conclude that in the absence of Bcd, Erk-induced endoderm specification is complete, with all cells adopting a posterior morphogenesis program during gastrulation. Because of their ability to drive coordinated tissue movements at any embryonic position in response to light, OptoSOS-*bcd* embryos may prove useful in future studies

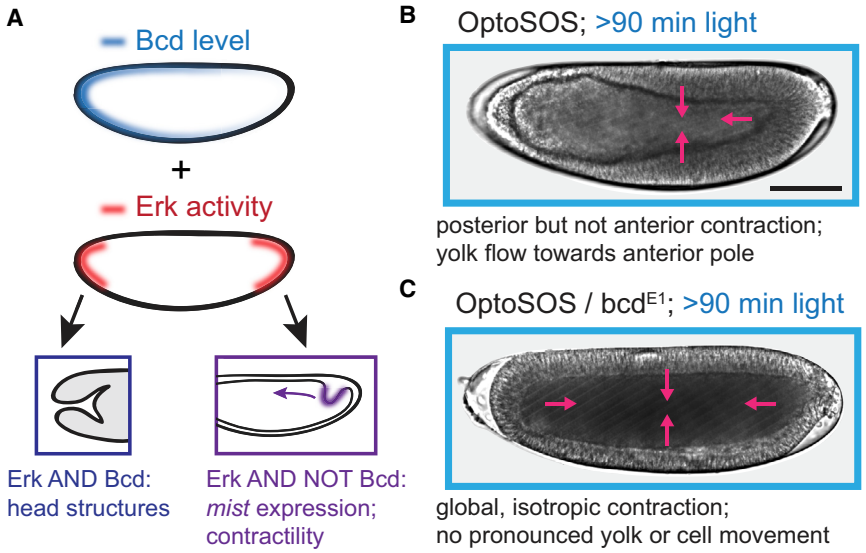

Figure 2. Erk-Induced Contractility Is Global and Isotropic in the Absence of Bcd Activity

(A) Schematic illustrating the conceptual model that anterior Bcd activity may be combinatorially interpreted with Erk to repress posterior fates, including light-induced tissue contractility.

(B and C) Differential interference contrast (DIC) images of gastrulating OptoSOS embryos (B) and OptoSOS-*bcd* embryos (C) that were stimulated with at least 90 min of continuous light prior to gastrulation (see also Video S4). In (B), contraction extends everywhere except the anterior pole (purple arrows), leading to large-scale cell rearrangements toward the posterior pole and yolk movement toward the anterior pole. In (C), contraction is isotropic (purple arrows) and blocks virtually all tissue reorganization. Scale bar, 100 μm.

that aim to quantitatively relate mechanical forces to tissue morphogenesis (Izquierdo et al., 2018; Guglielmi et al., 2015).

Distinct Erk Dynamics Trigger Cells to Adopt Either Lateral or Posterior Cell Fates

Although our experiments so far focused on adoption of posterior fates, they also reveal a puzzling dual role for Erk along the embryo's lateral surface. In wild-type embryos, lateral Erk activity is required to form intermediate neuroblasts, a population of ectoderm-derived neuronal progenitors (Schweitzer et al., 1995). These cells exhibit high levels of endogenous Erk signaling but do not normally contract at the start of gastrulation. Yet light-stimulated Erk is still able to induce their contraction and posterior gene expression (Figure 1). How can Erk signaling specify two distinct responses from the same cell population?

We hypothesized that the distinct responses are the result of dynamic control. According to such a model, differences in some feature of Erk activity over time would select between lateral and posterior fates. Intriguingly, prior studies revealed that Erk dynamics differ between the embryo's termini and lateral regions in two ways. First, the developmental timing of Erk activation differs: at the posterior, Erk signaling is initiated during the earliest nuclear cycles, whereas lateral Erk is activated shortly before gastrulation (Lim et al., 2015). Second, the duration of Erk signaling also differs: lateral Erk is activated in a transient 30-min pulse, whereas terminal signaling is sustained for over 1 h (Lim et al., 2015; Coppey et al., 2008).

To determine whether the timing or duration of Erk activity influences cell fates, we systematically varied the light inputs delivered to OptoSOS embryos. We stimulated 288 individual OptoSOS embryos of varying ages with either 30, 45, 60, or 120 min of blue light and imaged their progression through gastrulation (Figures S3A and S3B). Far-red (740 nm) light was used for imaging to avoid additional optogenetic stimulation, and embryos were scored based on their gastrulation phenotypes, which indicated the size of the domain of contractile posterior endoderm. The results of this experiment are shown in Figure 3A.

All embryos that were subjected to a 30-min pulse of light gastrulated normally (Figure 3A, bottom). However, these embryos were not completely unaffected by Erk: cuticle preparations revealed abdominal segment fusions similar to those induced by gain-of-function MEK mutants, likely due to disruption of the segment-patterning gene network through increased expression of the terminal gap genes *tll* and *hkb* (Figure S3C). At the other extreme, 60 min of illumination triggered a full contractile response in the majority of illuminated embryos, with 100% of embryos contracting after 120 min of light (Figure 3A, top). Lastly, a 45-min pulse of light caused a majority of embryos to adopt an intermediate phenotype similar to what is observed in embryos expressing a constitutively active Torso receptor (Tor^{GOF} embryos): a partial expansion of the posterior domain and incomplete germ band extension, leading to lethality shortly after gastrulation (Figure 3A, middle; for details of this phenotype, see also STAR Methods; Figures S3D and S3E; Video S6). Although the mechanism underlying partial expansion of the posterior domain is not completely clear, we conjecture that it may arise from the combined dose of Erk activity summed from our light input and the endogenous gradient, which is initially broad and subsequently narrows to the poles (Coppey et al., 2008).

These observations were highly informative about how Erk activity is interpreted into a cell fate response. The same light intensity was used for all experiments, yet led to outcomes varying from normal gastrulation to global tissue contraction. Thus, cell fate is not simply encoded in the amplitude of Erk activation, as would be expected for a classical morphogen. The developmental time at which light was delivered also had no clear effect provided it was delivered before gastrulation and after nuclear cycle 10, when nuclei are at the embryo surface and are presumably first able to respond to Erk signaling. This insensitivity to timing rules out the possibility that posterior fates are only established during a specific temporal window. In contrast, the duration of Erk activation was quite predictive of gastrulation and cuticle phenotypes (Figures 3B and S4). It thus appears that some feature of Erk activation that correlates with its duration—such as its pulse length, total time on, or area under the curve—is sufficient to program gut endoderm at non-terminal positions.

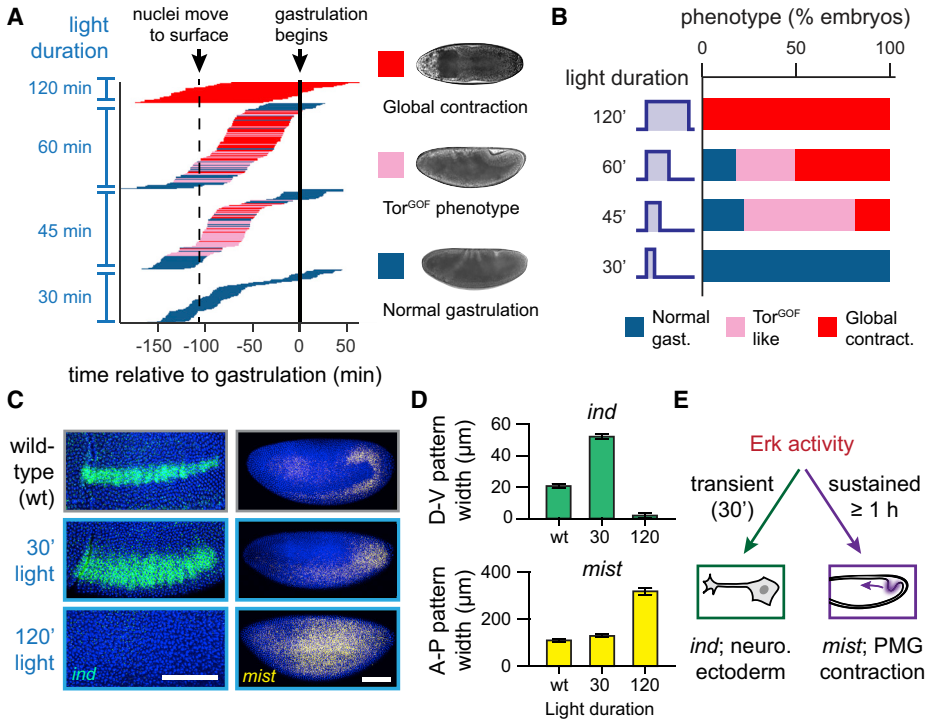

Figure 3. Erk Dynamics Control a Cell-Fate Switch in the Early *Drosophila* Embryo

(A) Experimental data showing the phenotypes of 288 individual OptoSOS embryos that were imaged after stimulating with light at various developmental times and with different durations of light (see Figures S3A and S3B for experimental workflow). Each horizontal line represents 1 DIC-imaged embryo, and the length and position of the line represents the time of light application. The color of each line represents its gastrulation phenotype according to the legend shown. The time at which stimulation was applied was deduced after aligning all embryos at the experimentally measured start of gastrulation (solid line); the time of nuclei moving to the surface (dashed line) is approximate and shown for reference.

(B) The fraction of embryos exhibiting each gastrulation phenotype is plotted as a function of stimulus duration for the embryos in (A).

(C) Representative images of RNA FISH for *ind* (at the start of gastrulation) and *mist* (just prior to gastrulation) at three stages: histone-GFP ("wild-type") embryos and then as OptoSOS embryos that were illuminated with 450 nm light for the indicated durations. Scale bars, 100 μm.

(D) Quantification of the width of each expression pattern (D–V for *ind*; A–P for *mist*) for embryos stimulated as in (C).

(E) Conceptual model of how Erk-induced neurogenic and contractile fates are distinguished. Transient Erk activity gives rise to *ind* expression and neurogenic fates, while sustained activity programs *mist* expression and tissue contractility.

For Erk dynamics to truly control a cell fate switch, cells must be capable of mounting distinct responses in response to different temporal signals. Thus far, we only probed a single fate: the ability for sustained Erk signaling to induce posterior fates throughout the embryo. If dynamic control governs the switch between posterior and lateral fates, then a short pulse of light-activated Erk would be expected to expand the population of intermediate neuroblasts, with a long pulse switching the same cells to endodermal fates. To test this prediction, we stimulated OptoSOS cells with 0, 30, or 120 min of light and stained for *intermediate neuroblasts defective* (*ind*), a gene that marks the Erk-dependent neuroblast population at lateral embryonic positions, and *mist*, which marks posterior contractile cells. Stimulation with a transient, 30-min light pulse expanded *ind* expression dorsally but did not induce *mist* expression in those cells (Figure 3C). In contrast, 120 min of light completely abolished *ind* expression, instead inducing *mist* expression in the same lateral cells (Figure 3C). We quantified the expansion of *ind* and *mist* patterns, finding that transient illumination could expand the *ind* stripe by almost 3-fold along the dorsoventral axis without substantially altering the extent of the *mist* pattern; conversely, *ind* was abolished and *mist* was expanded along the anteroposterior axis in response to sustained illumination (Figure 3D).

It is noteworthy that in these experiments we only observed a widening of the lateral stripe of intermediate neuroblasts, not global induction of *ind* expression similar to that which we observed for endoderm expansion. This spatial restriction is to be expected, due to the well-established co-requirement of Erk and intermediate levels of Dorsal for *ind* expression (Lim et al., 2013). After transient light stimulation, the expanded domain of Erk activity overlaps the region of Dorsal expression in a thicker lateral stripe. In sum, optogenetic stimulation and gene expression analyses reveal that lateral cells can be switched between three outcomes—no Erk-triggered response, neurogenic endoderm, and gut ectoderm—simply by increasing the duration of activity of a single signaling pathway (Figure 3E).

Cell Responses Are Triggered by the Cumulative Dose of Erk Signaling

What feature of Erk activity over time is sensed by cells to determine their fate? Differences in signaling dynamics have long been hypothesized to select among Erk-dependent cell fates

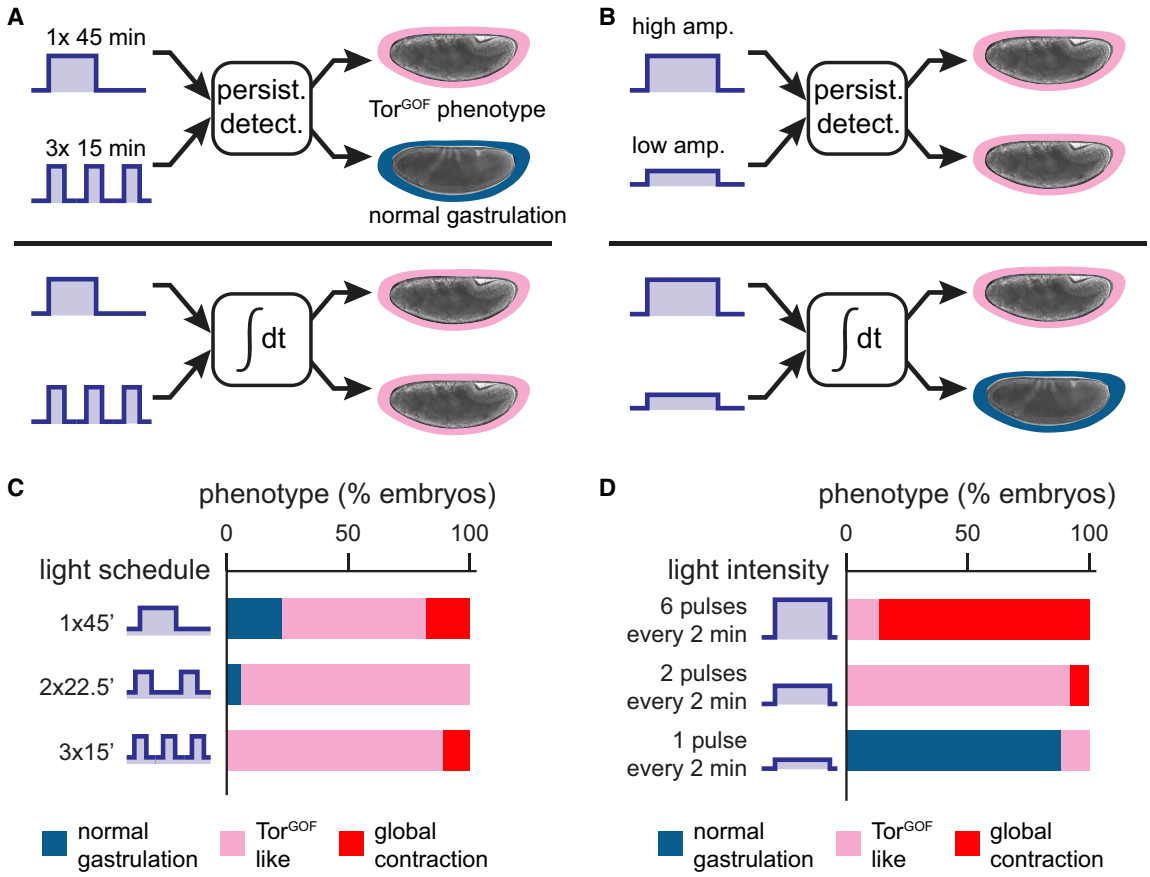

Figure 4. Embryo Phenotypes Are Determined by the Cumulative Load of Erk Signaling

Gastrulation phenotypes may be triggered by two classes of dynamic decoders, a persistence detector or a cumulative load sensor. These two decoders can be discriminated by their responses to certain light patterns.

(A) A persistence detector could be triggered by a single light bolus, but not when that signal is partitioned into multiple short, light bouts; a cumulative load sensor would fire in response to both equal-dose inputs.

(B) A cumulative load sensor could be triggered by high-intensity illumination but not by a lower-intensity input of the same duration; a persistence detector would respond similarly to both equal-duration inputs.

(C) Gastrulation phenotypes for the light schedules in (A). OptoSOS embryos were exposed to a single 45-min pulse of blue light or to the same 45-min dose split into 2 or 3 equal pulses and delivered over a 90-min period. Each bar represents the percentage of embryos exhibiting different gastrulation phenotypes according to the legend shown.

(D) Gastrulation phenotypes for the light schedules shown in (B). OptoSOS embryos were exposed to different numbers of 1-s light pulses every 2 min for a total of 60 min. Bars represent phenotypes as in (C).

(Marshall, 1995; Bishop et al., 1994), and at least two distinct mechanisms for decoding Erk dynamics have been proposed. The classic model is that of a persistence detector, where downstream genes sense the duration of a single Erk pulse (as is thought to be the case for gene products such as *c-fos*) (Nakakuki et al., 2010; Murphy et al., 2004). An alternative model is that of cumulative load detection, where distinct fates are triggered when the total integrated signal crosses a threshold (Gillies et al., 2017; Hannanta-Anan and Chow, 2016). Reasoning that these different types of dynamic decoding could be distinguished by their responses to different time-varying stimuli, we next set out to assess cell fates after different light schedules (Figures 4A and 4B).

We reasoned that a cumulative load sensor and a persistence detector would behave differently if the same light dose was delivered as a single bolus or multiple short pulses (Figure 4A), inputs which share the same cumulative load but have different pulse durations. We chose a total illumination time of 45 min because it induces the Tor^{GOF}-like phenotype, an intermediate outcome that could be altered either by an increase or decrease in the strength of signaling. Over a 90-min time period prior to gastrulation, we stimulated embryos with either a single 45-min pulse, two 22.5-min pulses separated by a 45-min gap, or three 15-min pulses separated by 15-min gaps. Regardless of the pulse schedule used, a majority of embryos in each stimulus condition adopted an identical Tor^{GOF} phenotype, consistent with cumulative load but not persistence detection determining the gut endoderm fate switch (Figure 4C). These data also show that the accumulated Erk dose is accurately "remembered" even across multiple nuclear division cycles: two 22.5-min pulses separated by a 45-min gap induce the same phenotype as a single 45-min light dose. We obtained

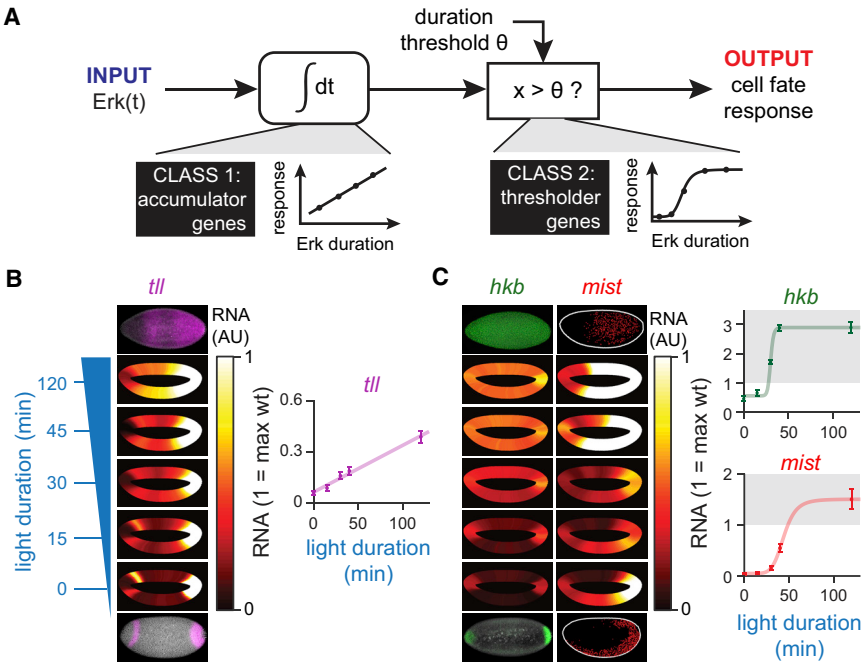

Figure 5. Distinct Target Genes Act as Accumulators and Thresholders of Erk Activity

(A) Model of cumulative load sensing by an accumulator and thresholder circuit. An accumulator node would increase linearly in response to Erk activity until a critical threshold θ is reached, at which point a thresholder node would turn on in a switch-like fashion.

(B and C) Analysis of RNA FISH data from Opto-SOS embryos exposed to varying durations of blue light and stained for (B) *tll* and (C) *hkb*/*mist*. The mean expression levels around the surface of the embryo are shown in each embryo-shaped heatmap; at least 50 embryos were analyzed for each light duration in (B) and (C). The heatmaps are saturated so that the white color is equivalent to the maximum level seen in a wild-type embryo (full plots are shown in Figure S5). For the inset plots in (B) and (C), the gene expression of cells at the dorsal-most cap of the embryo is plotted as a function of light duration, where a value of 1 is set to the maximum RNA signal seen in wild-type embryos.

similar results using a second phenotypic assay: cuticle preparations to assess segmentation of the body plan (Figure S4A). In this assay, a similar proportion of embryos exhibited segment fusions in response to 15 min of continuous illumination or three 5-min pulses delivered over 90 min, suggesting that the segmentation gene network is also sensitive to the total Erk dose. Additionally, a majority of embryos stimulated with a single 45-min pulse or three 15-min pulses lacked cuticle structures altogether (Figure S4A), consistent with these embryos' failure to properly gastrulate (Figure 4C).

To further probe whether the total dose of Erk controls embryonic phenotypes, we reasoned that different ways of varying the dose should elicit similar phenotypes, such as by varying signaling duration at a fixed amplitude or varying amplitude over a fixed duration (Figure 4B). To attain intermediate Erk amplitudes, we adopted a strategy of varying the number of brief, bright light pulses delivered every 2 min. We previously showed that the ERK pathway gradually turns on and off over ~4 min, so that these fast, frequent stimuli are averaged to an intermediate activity level (Toettcher et al., 2013). This strategy, termed pulse width modulation, is easily transferable between assays with different light sources or physical configurations where intensity is difficult to control and has been applied in a growing number of optogenetic contexts (Chen et al., 2017; Davidson et al., 2013).

Indeed, we found that varying the effective intensity of a 60-min light stimulus resulted in the same sequence of gastrulation phenotypes as when we varied the duration of a single pulse (compare Figure 4D to Figures 3A and 3B). These data are also consistent with the behavior of MEK^{GOF} and Tor^{GOF} mutant embryos, which activate Erk to a low, constant level away from the termini (Figures S1A–S1C) and induce segmentation and gastrulation phenotypes that are similar to those obtained by 30- or 45-min light pulses (Figures S3D, S3E, and S4B). We thus conclude that the decision to adopt posterior, contractile cell fates is primarily controlled by the overall dose (i.e., duration × time) of Erk signaling.

Distinct Erk Target Genes Accumulate Gradually or Are Triggered above a Stimulus Threshold

How might the cumulative load of a signal trigger an all-or-none cell fate switch? The simplest model requires two signal processing components, an "accumulator" and "thresholder" (Figure 5A). The accumulator component passively integrates Erk signal over time, providing memory of the total amount of Erk signaling that has been delivered. The thresholder would act downstream of the accumulator, comparing the accumulated signal to a fixed threshold and triggering a response only after the threshold is crossed. Such a model would predict two distinct behaviors among Erk-dependent genes: some might act as accumulators whose levels rise in linear proportion to the total light input, whereas others would act as thresholders that respond abruptly above a stimulus threshold.

To test if distinct target genes act as accumulators and thresholders of Erk signaling, we stained for *tll*, *hkb*, and *mist* in response to different durations of light stimulation in at least 50 embryos per condition. We then quantified RNA levels around the circumference of each embryo in order to obtain a quantitative map of target gene induction at all anterior-posterior and dorsal-ventral coordinates (expression heatmaps shown in Figures 5B and 5C, with line graphs plotted in Figure S5). To ascertain how gene expression varies with light dose, we analyzed a region on the dorsal surface at 50% embryo length (Figures 5B and 5C, right panels). This region was chosen because wild-type embryos exhibit no detectable Erk activity or target gene expression there, so all activity is solely a function of our light stimulus. We found that *tll* responded as would be predicted for an accumulator gene: its levels increased linearly as a function of the duration of Erk signaling (Figure 5B). In contrast, *hkb* and *mist* acted as threshold genes that turned on after 30 min

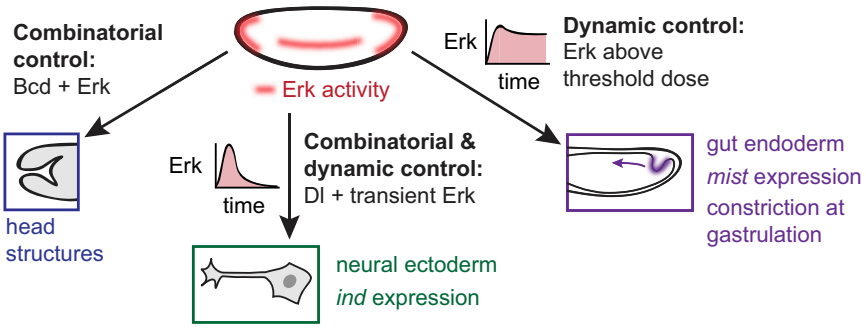

Figure 6. A Conceptual Model of Erk-Dependent Cell Fate Control in the Early Embryo

At the anterior pole, the presence of Bcd prevents light-induced endoderm specification and tissue contraction, regardless of Erk dose. Along the ventral midline, transient Erk activity induces cells to adopt an intermediate neuroblast fate, provided that they are also exposed to intermediate Dorsal signaling. In the posterior, sustained Erk activity induces posterior midgut differentiation, contraction at gastrulation, and suppression of neurogenic fates. This model reveals that lateral cells may be switched between two fates, posterior midgut and neurogenic ectoderm—depending on their cumulative dose of Erk activity.

and 45 min of signaling, respectively (Figure 5C; for comparison of linear and ultrasensitive model fits, see Figures S5E and S5F). The difference we observe between *tll* and *hkb* correlates well with prior mutant data showing that in embryos with weak terminal signaling, *hkb* expression is lost before *tll* expression (Furriols et al., 1996). The threshold duration at which *mist* is switched on (between 45 and 60 min) coincides exactly with the threshold for large-scale tissue contractility, consistent with *mist*'s essential role in this process.

Although our data reveals some candidate accumulator and thresholder nodes, a fully defined transcriptional network for Erk dynamic interpretation remains to be elucidated. Other attractive candidates for these functions also exist, including the Erk-regulated transcriptional repressor Capicua (Cic). In the now-classic model of terminal signaling, Cic is phosphorylated by Erk, leading to Cic nuclear export and degradation followed by de-repression of *tll* and *hkb* (Jiménez et al., 2000). It is possible that the gradual loss of Cic thus integrates the total Erk dose, triggering gene expression only after its removal. However, a few lines of evidence suggest that this is not the whole story. The gastrulation phenotype of *cic*-null embryos is less severe than that of illuminated OptoSOS embryos, suggesting that Erk drives further posteriorization independently of Cic. Also, staining for Cic protein in globally illuminated OptoSOS embryos or GOF mutant embryos reveals that Cic is not fully degraded even in regions where *tll* and *hkb* expression are expressed at high, uniform levels (Johnson et al., 2017; de las Heras and Casanova, 2006).

DISCUSSION

Through a combination of genetic perturbations and time-varying optogenetic stimuli, the current study begins to define a model for how Erk is capable of programming three distinct cell fates for the early embryo (Figure 6). At the posterior, sustained Erk signaling induces gut endoderm, tissue that is characterized by expression of the Fog/Mist receptor-ligand pair, which leads to apical constriction and tissue invagination. The boundary of this tissue is determined by the total Erk dose, and sustained Erk activity at almost any embryonic position is sufficient to trigger gut endoderm gene expression and contractility. A notable exception is the anterior pole, where the combination of Bcd and Erk switches cells to anterior fates. In the middle of the embryo, the combination of transient Erk and Dorsal normally induces the formation of ectoderm-derived neuroblasts, a fate that can be overridden by additional, ectopic Erk activity. By isolating the Erk pathway and titrating the inputs we deliver, we further show that some cells in the embryo can adopt three distinct responses at different signaling thresholds. Lateral cells shift from no response to form intermediate neuroblasts (characterized by *ind* expression) or gut endoderm (marked by *mist* expression and contractility) as a single input parameter—the duration of Erk signaling—is increased. These three transitions are reminiscent of the requirements that define a morphogen, a substance whose concentration determines multiple distinct fates (Gurdon et al., 1998). Yet in the case of Erk, it is signaling dynamics, not instantaneous concentration, which is interpreted into a cellular response.

In contrast to the now-classic models for how Erk dynamics are decoded in cultured cells (Nakakuki et al., 2010; Murphy et al., 2004), we find that the early *Drosophila* embryo does not read the duration of a single persistent stimulus but rather senses the cumulative load of Erk signaling. Two lines of evidence support this conclusion. First, the same overall Erk dose can be delivered in a single bolus or divided into discrete pulses spread out over a 2-h window, leading to the same effect. Second, long low-amplitude light stimuli (as well as gain-of-function mutants that activate Erk to low levels) achieve the same phenotypes as short high-amplitude light pulses. But does this distinction between duration and cumulative load sensing matter? We would argue that it is quite important, as the putative network architectures that perform these two signal processing functions can be quite different. Persistence detection is thought to rely on network motifs like the coherent feedforward loop (Mangan and Alon, 2003), whereas cumulative load detection can be implemented by combining long-term integration with an ultrasensitive downstream step. Obtaining the dynamic input-output response of a biological network can thus be a crucial first step toward a complete understanding of its network architecture and subsequent identification of molecular components (Mettetal et al., 2008). Such insights are sorely needed, as we still broadly lack a mechanistic understanding of how signaling pathway activity is decoded into precise, reproducible patterns of gene expression.

There are still many unresolved questions regarding Erk-dependent cell fate choices in the early embryo. We have shown Bcd is sufficient to prevent posterior fates at the anterior pole, but future work must be done to dissect how Erk dynamics interact with the Bcd gradient to pattern the formation of different anterior structures. A complete picture of anterior fate choices

may benefit from precise control over both Bcd and Erk using multi-color optogenetics (Huang et al., 2017). Moreover, the Erk-dependent terminal gap genes *tll* and *hkb* do much more than specify terminal fates and participate in complex interactions with other gap and segmentation genes. Indeed, we find that brief 15–30 min light stimuli do not affect gastrulation but lead to abdominal segment fusion, suggesting that the segmentation gene network is quite sensitive to perturbations in the spatiotemporal profile of Erk signaling. The use of light to deliver quantitative spatial and temporal perturbations to gap gene expression could prove instrumental for a deeper understanding of the segmentation circuit (Schroeder et al., 2004).

The Ras/Erk pathway is only one of many signaling outputs from receptor tyrosine kinases (RTKs), and in general, it remains an open question whether light-induced Erk fully reproduces all the nuances of receptor-level stimulation. To further probe this question in the early embryo, we tested whether OptoSOS stimulation recapitulates a classic genetic epistasis result: in embryos expressing a gain-of-function Torso RTK, loss of *tll* can suppress the Tor^{GOF} phenotype (Klingler et al., 1988). Indeed, we found that the expected proportion of OptoSOS-*tll* treated with 45 min of light exhibit the *tailless* phenotype, not the Tor^{GOF}-like phenotype normally observed in OptoSOS embryos (Figure S4C; STAR Methods). Interestingly, suppression is lost at higher light doses, suggesting that sufficiently strong Erk activity can posteriorize embryos even in the absence of *tll* (Figure S4C). Looking forward, the recent development of light-controlled RTKs (Dine et al., 2018; Grusch et al., 2014; Kim et al., 2014) opens the door to a full, systematic comparison between stimulation at the levels of the receptor versus Ras, and we eagerly await a quantitative comparison between these approaches.

The relationship between Erk dynamics and cellular responses has long been studied in cultured mammalian cells (Marshall, 1995; Bishop et al., 1994). Here, we find that principles of dynamic control also operate to control Erk-dependent cell fates in a developing organism. We would argue that the early *Drosophila* embryo is an ideal model system for dissecting dynamic control: cell fates specification occurs within 3 h and is highly reproducible between embryos, gastrulation movements can be observed by bright-field microscopy and provide a spatially-localized readout of cell fate, the list of "downstream" candidates for decoding dynamics is limited to a few dozen active zygotic genes in the early embryo (De Renzis et al., 2007), and the combination of optogenetic and classical genetic tools enable complex perturbations of network components. Moreover, Erk signaling in the early embryo is likely to be only one of many examples of dynamic cell fate control *in vivo*. The approaches outlined here could prove useful in many additional contexts for dissecting how developmental cell fates are specified.

STAR★METHODS

Detailed methods are provided in the online version of this paper and include the following:

- KEY RESOURCES TABLE
- CONTACT FOR REAGENT AND RESOURCE SHARING
- EXPERIMENTAL MODEL AND SUBJECT DETAILS
  - *Drosophila melanogaster* Stocks
- METHOD DETAILS
  - Light Illumination and Light Stimulation Experiments
  - Microscopy
  - Immunostaining and Fluorescence *In Situ* Hybridization
- QUANTIFICATION AND STATISTICAL ANALYSIS
  - Analysis of Myosin Timing
  - Analysis of Gene Expression Profiles
  - Analysis of Gastrulation Phenotypes
  - Analysis of OptoSOS-tll Phenotypes
  - Comparison of Models Fits to Data of Gene Expression versus Light Duration
- DATA AND SOFTWARE AVAILABILITY

SUPPLEMENTAL INFORMATION

Supplemental Information includes five figures and six videos and can be found with this article online at https://doi.org/10.1016/j.devcel.2019.01.009.

ACKNOWLEDGMENTS

We thank all members of the Toettcher Lab for helpful comments, as well as Stas Shvartsman and Eric Wieschaus for their suggestions and insights throughout the study. Yuji Yamazaki kindly provided the *mist* RNA probe. H.E.J. was supported by the NIH Ruth Kirschstein fellowship F32GM119297. This work was also supported by NSF CAREER Award 1750663 (to J.E.T.). We also thank Dr. Gary Laevsky and the Molecular Biology Microscopy Core, which is a Nikon Center of Excellence, for microscopy support.

AUTHOR CONTRIBUTIONS

H.E.J. and J.E.T. conceived and designed the project and wrote the manuscript. H.E.J. performed all experiments.

DECLARATION OF INTERESTS

The authors declare no competing interests.

Received: June 21, 2018
Revised: November 27, 2018
Accepted: January 4, 2019
Published: February 11, 2019

REFERENCES

Asokan, S.B., Johnson, H.E., Rahman, A., King, S.J., Rotty, J.D., Lebedeva, I.P., Haugh, J.M., and Bear, J.E. (2015). Mesenchymal chemotaxis requires selective inactivation of myosin II at the leading edge via a non-canonical PLCγ/PKCα pathway. Dev. Cell *31*, 747–760.

Bishop, J.M., Capobianco, A.J., Doyle, H.J., Finney, R.E., McMahon, M., Robbins, S.M., Samuels, M.L., and Vetter, M. (1994). Proto-oncogenes and plasticity in cell signaling. Cold Spring Harb. Symp. Quant. Biol. *59*, 165–171.

Bugaj, L.J., Sabnis, A.J., Mitchell, A., Garbarino, J.E., Toettcher, J.E., Bivona, T.G., and Lim, W.A. (2018). Cancer mutations and targeted drugs can disrupt dynamic signal encoding by the Ras-Erk pathway. Science *361*, https://doi.org/10.1126/science.aao3048.

Chen, F.B., Budgett, D.M., Sun, Y., Malpas, S., McCormick, D., and Freestone, P.S. (2017). Pulse-width modulation of optogenetic photo-stimulation intensity for application to full-implantable light sources. IEEE Trans. Biomed. Circuits Syst. *11*, 28–34.

Coppey, M., Boettiger, A.N., Berezhkovskii, A.M., and Shvartsman, S.Y. (2008). Nuclear trapping shapes the terminal gradient in the Drosophila embryo. Curr. Biol. *18*, 915–919.

Davidson, E.A., Basu, A.S., and Bayer, T.S. (2013). Programming microbes using pulse width modulation of optical signals. J. Mol. Biol. *425*, 4161–4166.

Dawes-Hoang, R.E., Parmar, K.M., Christiansen, A.E., Phelps, C.B., Brand, A.H., and Wieschaus, E.F. (2005). folded gastrulation, cell shape change and the control of myosin localization. Development *132*, 4165–4178.

de las Heras, J.M., and Casanova, J. (2006). Spatially distinct downregulation of Capicua repression and tailless activation by the Torso RTK pathway in the Drosophila embryo. Mech. Dev. *123*, 481–486.

De Renzis, S., Elemento, O., Tavazoie, S., and Wieschaus, E.F. (2007). Unmasking activation of the zygotic genome using chromosomal deletions in the Drosophila embryo. PLoS Biol. *5*, e117.

Dine, E., Gil, A.A., Uribe, G., Brangwynne, C.P., and Toettcher, J.E. (2018). Protein phase separation provides long-term memory of transient spatial stimuli. Cell Syst. *6*, 655–663.

Driever, W., Siegel, V., and Nüsslein-Volhard, C. (1990). Autonomous determination of anterior structures in the early Drosophila embryo by the bicoid morphogen. Development *109*, 811–820.

Furriols, M., Sprenger, F., and Casanova, J. (1996). Variation in the number of activated torso receptors correlates with differential gene expression. Development *122*, 2313–2317.

Gillies, T.E., Pargett, M., Minguet, M., Davies, A.E., and Albeck, J.G. (2017). Linear integration of ERK activity predominates over persistence detection in Fra-1 regulation. Cell Syst. *5*, 549–563.

Goyal, Y., Jindal, G.A., Pelliccia, J.L., Yamaya, K., Yeung, E., Futran, A.S., Burdine, R.D., Schüpbach, T., and Shvartsman, S.Y. (2017). Divergent effects of intrinsically active MEK variants on developmental Ras signaling. Nat. Genet. *49*, 465–469.

Grimm, O., Sanchez Zini, V.Z., Kim, Y., Casanova, J., Shvartsman, S.Y., and Wieschaus, E. (2012). Torso RTK controls Capicua degradation by changing its subcellular localization. Development *139*, 3962–3968.

Grusch, M., Schelch, K., Riedler, R., Reichhart, E., Differ, C., Berger, W., Inglés-Prieto, Á., and Janovjak, H. (2014). Spatio-temporally precise activation of engineered receptor tyrosine kinases by light. EMBO J. *33*, 1713–1726.

Guglielmi, G., Barry, J.D., Huber, W., and De Renzis, S. (2015). An optogenetic method to modulate cell contractility during tissue morphogenesis. Dev. Cell *35*, 646–660.

Gurdon, J.B., Dyson, S., and St Johnston, D. (1998). Cells' perception of position in a concentration gradient. Cell *95*, 159–162.

Hannanta-Anan, P., and Chow, B.Y. (2016). Optogenetic control of calcium oscillation waveform defines NFAT as an integrator of calcium load. Cell Syst. *2*, 283–288.

Huang, A., Amourda, C., Zhang, S., Tolwinski, N.S., and Saunders, T.E. (2017). Decoding temporal interpretation of the morphogen bicoid in the early Drosophila embryo. Elife *6*, https://doi.org/10.7554/eLife.26258.

Hunter, C., and Wieschaus, E. (2000). Regulated expression of nullo is required for the formation of distinct apical and basal adherens junctions in the Drosophila blastoderm. J. Cell Biol. *150*, 391–401.

Imayoshi, I., Isomura, A., Harima, Y., Kawaguchi, K., Kori, H., Miyachi, H., Fujiwara, T., Ishidate, F., and Kageyama, R. (2013). Oscillatory control of factors determining multipotency and fate in mouse neural progenitors. Science *342*, 1203–1208.

Izquierdo, E., Quinkler, T., and De Renzis, S. (2018). Guided morphogenesis through optogenetic activation of Rho signalling during early Drosophila embryogenesis. Nat. Commun. *9*, 2366.

Jiménez, G., Guichet, A., Ephrussi, A., and Casanova, J. (2000). Relief of gene repression by torso RTK signaling: role of capicua in Drosophila terminal and dorsoventral patterning. Genes Dev. *14*, 224–231.

Johnson, H.E., Goyal, Y., Pannucci, N.L., Schüpbach, T., Shvartsman, S.Y., and Toettcher, J.E. (2017). The spatiotemporal limits of developmental erk signaling. Dev. Cell *40*, 185–192.

Kim, N., Kim, J.M., Lee, M., Kim, C.Y., Chang, K.Y., and Heo, W.D. (2014). Spatiotemporal control of fibroblast growth factor receptor signals by blue light. Chem. Biol. *21*, 903–912.

Klingler, M., Erdélyi, M., Szabad, J., and Nüsslein-Volhard, C. (1988). Function of torso in determining the terminal anlagen of the Drosophila embryo. Nature *335*, 275–277.

Kosman, D., Mizutani, C.M., Lemons, D., Cox, W.G., McGinnis, W., and Bier, E. (2004). Multiplex detection of RNA expression in Drosophila embryos. Science *305*, 846.

Lim, B., Dsilva, C.J., Levario, T.J., Lu, H., Schüpbach, T., Kevrekidis, I.G., and Shvartsman, S.Y. (2015). Dynamics of inductive ERK signaling in the Drosophila embryo. Curr. Biol. *25*, 1784–1790.

Lim, B., Samper, N., Lu, H., Rushlow, C., Jiménez, G., and Shvartsman, S.Y. (2013). Kinetics of gene derepression by ERK signaling. Proc. Natl. Acad. Sci. USA *110*, 10330–10335.

Mangan, S., and Alon, U. (2003). Structure and function of the feed-forward loop network motif. Proc. Natl. Acad. Sci. USA *100*, 11980–11985.

Manning, A.J., Peters, K.A., Peifer, M., and Rogers, S.L. (2013). Regulation of epithelial morphogenesis by the G protein-coupled receptor mist and its ligand fog. Sci. Signal. *6*, ra98.

Marshall, C.J. (1995). Specificity of receptor tyrosine kinase signaling: transient versus sustained extracellular signal-regulated kinase activation. Cell *80*, 179–185.

Martin, A.C., Kaschube, M., and Wieschaus, E.F. (2009). Pulsed contractions of an actin-myosin network drive apical constriction. Nature *457*, 495–499.

Mettetal, J.T., Muzzey, D., Gómez-Uribe, C., and van Oudenaarden, A. (2008). The frequency dependence of osmo-adaptation in Saccharomyces cerevisiae. Science *319*, 482–484.

Murphy, L.O., MacKeigan, J.P., and Blenis, J. (2004). A network of immediate early gene products propagates subtle differences in mitogen-activated protein kinase signal amplitude and duration. Mol. Cell. Biol. *24*, 144–153.

Nakakuki, T., Birtwistle, M.R., Saeki, Y., Yumoto, N., Ide, K., Nagashima, T., Brusch, L., Ogunnaike, B.A., Okada-Hatakeyama, M., and Kholodenko, B.N. (2010). Ligand-specific c-Fos expression emerges from the spatiotemporal control of ErbB network dynamics. Cell *141*, 884–896.

Nishimura, M., Inoue, Y., and Hayashi, S. (2007). A wave of EGFR signaling determines cell alignment and intercalation in the Drosophila tracheal placode. Development *134*, 4273–4282.

Purvis, J.E., and Lahav, G. (2013). Encoding and decoding cellular information through signaling dynamics. Cell *152*, 945–956.

Rahimi, N., Averbukh, I., Haskel-Ittah, M., Degani, N., Schejter, E.D., Barkai, N., and Shilo, B.Z. (2016). A WntD-dependent integral feedback loop attenuates variability in Drosophila Toll signaling. Dev. Cell *36*, 401–414.

Reuter, R., and Leptin, M. (1994). Interacting functions of snail, twist and huckebein during the early development of germ layers in Drosophila. Development *120*, 1137–1150.

Royou, A., Sullivan, W., and Karess, R. (2002). Cortical recruitment of nonmuscle myosin II in early syncytial Drosophila embryos: its role in nuclear axial expansion and its regulation by Cdc2 activity. J. Cell Biol. *158*, 127–137.

Schroeder, M.D., Pearce, M., Fak, J., Fan, H., Unnerstall, U., Emberly, E., Rajewsky, N., Siggia, E.D., and Gaul, U. (2004). Transcriptional control in the segmentation gene network of Drosophila. PLoS Biol. *2*, E271.

Schüpbach, T., and Wieschaus, E. (1986). Maternal-effect mutations altering the anterior-posterior pattern of the Drosophila embryo. Roux Arch. Dev. Biol. *195*, 302–317.

Schweitzer, R., Shaharabany, M., Seger, R., and Shilo, B.Z. (1995). Secreted Spitz triggers the der signaling pathway and is a limiting component in embryonic ventral ectoderm determination. Genes Dev. *9*, 1518–1529.

Toettcher, J.E., Weiner, O.D., and Lim, W.A. (2013). Using optogenetics to interrogate the dynamic control of signal transmission by the Ras/Erk module. Cell *155*, 1422–1434.

Wilson, M.Z., Ravindran, P.T., Lim, W.A., and Toettcher, J.E. (2017). Tracing information flow from Erk to target gene induction reveals mechanisms of dynamic and combinatorial control. Mol. Cell *67*, 757–769.

STAR★METHODS

KEY RESOURCES TABLE

REAGENT or RESOURCE	SOURCE	IDENTIFIER
Antibodies		
mouse anti-biotin	Jackson Immunoresearch	RRID: AB_2339006
sheep anti-digoxigenin	Roche	RRID: AB_514496
sheep anti-GFP	BioRad	RRID: AB_619712
rat anti-Fog	Gift from Wieschaus lab	N/A
Alexa Fluor conjugated secondary antibodies	Invitrogen	Various
Experimental Models: Organisms/Strains		
D. melanogaster: UAS-optoSOS	Johnson et al., 2017	N/A
D. melanogaster: 67;15	Hunter and Wieschaus, 2000	FlyBase: FBti0016179
D. melanogaster: Bcd^{E1}	Gift from Wieschaus lab	FlyBase: FBal0001080
D. melanogaster: Sqh-GFP	Gift from Wieschaus lab	FlyBase: FBti0073027
D. melanogaster: Tor^{D4021}	Schüpbach and Wieschaus, 1986	FlyBase: FBal0016921
D. melanogaster: Histone-GFP	Gift from Wieschaus lab	FlyBase: FBtp0012478
D. melanogaster: Tll^{L10}	Gift from Wieschaus lab	FlyBase: FBal0016889
D. melanogaster: UAS-MEK^{F53S}	Goyal et al., 2017	N/A
Software and Algorithms		
Fiji		http://fiji.sc
Matlab Code for analysis	This paper	https://github.com/h-e-j/Devcell2019

CONTACT FOR REAGENT AND RESOURCE SHARING

Further information and requests for resources should be directed to and will be fulfilled by the Lead Contact, Jared Toettcher (toettcher@princeton.edu).

EXPERIMENTAL MODEL AND SUBJECT DETAILS

Drosophila melanogaster Stocks

Transgenic UAS-optoSOS flies were produced as described previously (Johnson et al., 2017) by ϕC31-based integration at either CH III 68A4 or CH II 25C6 and are driven maternally using P(mata-GAL-VP16)mat15 for all experiments (Hunter and Wieschaus, 2000). Other stocks used include Bcd^{E1} (FBal0001080; a gift from Eric Wieschaus), Tor^{D4021} (FBal0016921), Sqh-GFP (FBti0073027), and UAS MEK F53S (Goyal et al., 2017). A Histone-GFP stock (FBtp0012478) was used for all wild-type comparisons in co-immunostaining experiments (Figures 1F–1H, 3C, and 3D). The Sqh-GFP;optoSOS fly was generated by double balancing and crossing Sqh-GFP with optoSOS CHIII. These flies were then crossed to 67;15 to drive optoSOS maternally. To generate OptoSOS embryos lacking maternal Bicoid we crossed bcd^{E1} double-balanced flies with optoSOS CH II double-balanced flies. These flies were then crossed to 67;15 bcd^{E1} *tsl* to drive optoSOS in the presence of the bcd^{E1} mutant maternally. To generate optoSOS-*tll* flies we recombined optoSOS with tll^{L10} (FBal0016889), screening for the *tll* cuticle phenotype, these were then crossed with 67;15 to drive optoSOS, with 25% of the progeny being homozygous for the mutation. All animal experiments were conducted under the oversight of Princeton's Institute Biosafety Committee.

METHOD DETAILS

Light Illumination and Light Stimulation Experiments

For all experiments carried out on bulk embryos (e.g. cuticle preparations), we used a custom-built panel of 30 individual 450 nm blue LEDs placed ~5 cm from the embryos and wrapped in foil. The light intensity at the sample location was measured with a MQ-510 Quantum light meter with separate sensor (Apogee Instruments) and determined to be approximately 1 mW / cm^2 of 450 nm light. Note that for all staining experiments comparing wild-type and light-induced OptoSOS stimulation (e.g. embryos in Figures 1 and 3), we co-incubated Histone-GFP (for wild-type) and OptoSOS embryos under the same light source, stained them together, and analyzed them separately *post facto* based on whether or not they expressed GFP.

Microscopy

Cuticles were prepared for imaging (Johnson et al., 2017) and imaged on Nikon Eclipse Ni at 10X objective using dark-field microscopy. In live fluorescence imaging experiments, embryos were dechorionated in 50% bleach for 2 min and rinsed in water before mounting and imaging. Microscopy of live and fixed fluorescent samples was performed using a Nikon A1 RS point-scanning confocal microscope (Princeton Confocal Microscopy Core).

DIC imaging was performed on our Nikon Eclipse Ti spinning-disk confocal microscope. A 740-760nm band-pass filter (Chroma) was placed in the bright-field illumination light path to prevent unwanted optogenetic stimulation during imaging. During times at which global stimulation was desired, the 750 nm band-pass filter was replaced with a 450 nm band-pass filter, and light intensity was adjusted to deliver $\sim$1 mW / cm^2 of 450 nm light. Light intensity was measured with a MQ-510 Quantum light meter with separate sensor (Apogee Instruments) placed at the sample location. Patterned optogenetic illumination was performed using a Mightex Polygon digital micromirror device using an X-Cite XLED 450-nm blue-light.

Immunostaining and Fluorescence *In Situ* Hybridization

Fluorescence in situ hybridization (FISH) and immunostaining was performed as described previously (Kosman et al., 2004). Primary antibodies used were rat anti-Fog (a gift from Eric Wieschaus), sheep anti-GFP (1:1,000, Bio-Rad), sheep anti-digoxigenin, (DIG) (1:125; Roche), and mouse anti-biotin (1:125; Jackson Immunoresearch). DAPI (1:10,000; Vector Laboratories) was used to stain for nuclei, and Alexa Fluor conjugates (1:500; Invitrogen) were used as secondary antibodies. For pairwise comparisons of wild-type and optogenetic stimulation, embryos were collected, stained, and imaged together under the same experimental conditions.

QUANTIFICATION AND STATISTICAL ANALYSIS

All statistical details (e.g. whether standard deviation or standard error is shown, the number of samples and replicates) are included in the figure legend for the corresponding experiment.

Analysis of Myosin Timing

All analyses of myosin activity began from maximum intensity-projected images of the gastrulating embryo (representative images are shown in Figures 1B and S2D). We separately validated that the myosin increases occurred solely on the apical surface by examining the original, un-projected 3D Z-stacks. Additionally, axial projections of our 3D image stacks enabled us to clearly separate the basal myosin accumulation during cellularization from apical myosin during gastrulation (Figure S2E). All analyses were performed in MATLAB® (The MathWorks, Natick, Massachusetts) and code is available on GitHub.

For analysis of the spatial domain and timing of apical myosin, images of Sqh-GFP embryos were analyzed in a method similar to (Asokan et al., 2015), adapted to the much larger size ''puncta'' that we observe on the embryo's apical surface compared to migrating mammalian cells. We took advantage of the observation that myosin accumulation occurs in small, intense spots on the apical surface of cells, with regions of low myosin accumulation between these puncta (Figure 1C). This enabled us to filter regions of myosin accumulation from the surrounding 'background' by subtracting a 36 μm^2 2-dimensional median filtered copy of the image, resulting in a background-subtracted image IMsub (Figure S2F; top panel). A mask of the embryo was also created by tmbryo structures. Together, these resulted in a binary mask of the embryo IMmask.

We next sought to process IMmask to obtain a 'ring' of apical pixels around the embryo in which to analyze myosin intensity. We first eroded the posterior-most portion of IMmask to exclude the non-contractile germ cells while preserving the contractile posterior epithelium. We then performed morphological erosion on IMmask using a 30 μm-radius disk, and subtracted it from whole embryo to create a 30 μm-radius 'ring' around the embryo; Figure S2F; bottom left panel. The average myosin intensity in IMsub was measured in angular bins around this ring at each time-point, thus creating a ''map'' of myosin intensity as a function of time and angle around the embryo (e.g. 0° = anterior; 90° = dorsal; 180° = posterior; Figure S2F; top right panel).

We then logically compared the intensity of this myosin map to its mean intensity, so as to obtain a binary map which revealed the times and positions at which myosin accumulation exceeded the mean across the experiment (Figure S2F; bottom right panel). We set the time of the first appearance of apical myosin (at any position) as t = 0, and the time delay of the first appearance of myosin in the other angular bins was calculated relative to this first-appearance time. The result for five light-stimulated OptoSOS embryos is shown in Figure 1D.

We also used the binary map to determine the length of embryo which apical myosin was induced. To do so, we queried the binary map for the maximum embryo-length at which myosin was observed at both the dorsal and ventral surface. This analysis resulted in an estimated extent of constriction of 88.4 ± 0.3% embryo length.

Analysis of Gene Expression Profiles

For analysis of the width of patterns in Figure 3D was measured in ImageJ (National Institutes of Health). For *ind*, a line was drawn in the across the pattern in the middle of the embryo and its width was calculated. An *ind* pattern width of zero was recorded if no pattern was observed. The distance of basal membrane from the edge of the embryo was used to estimate the age of the embryos; embryos were only analyzed if they shared widths with control embryos for which endogenous patterns were observed. To assess expansion of the *mist* pattern from the posterior pole, the length from posterior to anterior that mist was found on both

sides the embryo in NC12-14 (in various D-V orientations) was calculated. The ImageJ "Remove Outliers" function was used to remove non-specific FISH staining aggregates in images for display purposes.

For the data in Figures 5B and 5C, maximum-projected z-stacks of images were collected for FISH images of *tll*, *hkb*, and *mist* in NC12-14 embryos. These maximum-projected images were normalized to non-specific background staining, background subtracted, and analyzed in MATLAB. A mask of each embryo was created by k-means clustering the intensity image, and taking the lowest bin to be background. Morphological closing and the clearing of small structures was performed on this mask to heal minor discontinuities. The posterior-most portion of the mask was eroded to exclude germ cells, so that only the epithelial monolayer around the embryo was subjected to further analysis. The intensity of RNA staining in 9 μm wide contour around the edge around the embryo was calculated to avoid autofluorescence in the yolk. Intensity was totaled in each contour bin and normalized to the endogenous pattern. Due to the punctate expression of *mist* in pre-gastrulation embryos, puncta were segmented using 2-D median filtering (10 μm^2) and the number of puncta was counted, rather than using the intensity of *mist* staining directly. To obtain the dose response curves the middle dorsal surface bins of the contour (16% of the total contour length) were averaged and the average across all embryos was normalized to the average endogenous peak value.

Analysis of Gastrulation Phenotypes

From DIC movies of development, embryos were classified into three groups: global contraction, expanded PMG, and normal. Embryos were considered to exhibit "global contraction" when at least the posterior-most 40% of the embryo underwent contraction and the germ cells did not invaginate. "Expanded PMG" was classified by a lack of germband extension, or germ bands that retracted or stagnated immediately after PMG invagination, which was typically exaggerated in size (See Figure S3). Gastrulation was deemed "Normal" when both PMG invagination and germband extension occurred normally. Embryos which presented defects prior to gastrulation or were unfertilized were excluded from counts. For the bar graphs of Figures 3B and 4, embryos were included for analysis as long as light stimulus began at -140 min or later and was completed by -5 mins, where 0 min is taken as the time of gastrulation.

To confirm that short durations of light still had effects on embryos, such as those observed with GOF Mek mutations, we assayed cuticle phenotypes in response to a range of optogenetic stimuli and compared with mutants (Figures S4A and S4B). Indeed, optogenetic activation of Erk for as little as 10 minutes is capable of disrupting segmental patterning enough to induce cuticle fusions as are observed in the weaker GOF mutants, even though gastrulation is not significantly perturbed in either case. However, long durations of Erk result in a loss of segments entirely as we observed previously (Johnson et al., 2017), presumably do to the corresponding disruption of gastrulation. This is similar to mutants which activate Erk to higher levels, consistent with a model where the cumulative load of Erk dictates fates.

Analysis of OptoSOS-tll Phenotypes

For the analysis of cuticle phenotypes in Figure S4C, cuticles for each condition were classified into 3 groups, those which lacked segments, those which had 1-7 segments and lacked filzkörper (*tll*), and all others. The left hand side of the plot contains the expected values for *tll*, Tor^{D4021} and Tor^{D4021} in the presence of a *tll* LOF mutation. These values were calculated based on the assumption that *Tll* embryos should make up 25% of the population, with 4% of all embryos being unfertilized, there will be a small amount of empty cuticles. Likewise one would expect that this population would be the same population which does not lose all segments in the presence of Tor^{D4021}, with the remaining embryos having no segments.

Comparison of Models Fits to Data of Gene Expression versus Light Duration

For the model fits shown in Figures 5B and 5C, we compared fits to both linear and ultrasensitive models by computing the sum-of-squared error of the best fit curves in each case. The results are presented in Figures S5E and S5F. For the ultrasensitive model, we used the model

$$y = a\frac{t^n}{t^n + t_{1/2}} + b,$$

where y is the measured gene expression, a and b are the amplitude and offset of the gene expression intensities, t represents the duration of light stimulus, $t_{1/2}$ is the duration at which a half-maximal response is observed, and n is the Hill coefficient, representing the steepness of the response. For all fits we fixed $n = 10$, which we observed led to an excellent match for the switchlike reponses of *mist* and *hkb* gene expression. Our linear model was simply $y = at + b$, with a and b as the slope and offset and t the duration.

All fitting was performed in MATLAB using the lsqcurvefit function and a sum-of-squared-error (SSE) objective function. Example fits in the case of *hkb* gene expression are shown in Figure S5E, showing that a linear and first-order saturating model (which is identical to the ultrasensitive model but for $n = 1$) fit relatively poorly, whereas the ultrasensitive model fits well. The SSE for all linear and ultrasensitive fits is presented in Figure S5F, and the results from the best-fit model in each case is presented in bold.

DATA AND SOFTWARE AVAILABILITY

Analysis scripts are available at https://github.com/h-e-j/Devcell2019. Raw image data is available upon request.